Desalination and Water Treatment
www.deswater.com

doi: 10.5004/dwt.2019.23585

144 (2019) 384–392
March

Comparison of the uptake of methylene blue on α- and γ-MnO_2 nanomaterials

Van-Phuc Dinh[a,*], Thien-Hoang Ho[b], Thi-Thuy Luu[b], Hao-Nhien Vo[b], Thi-Thanh-Thao Do[b], Thi-Ha Trinh[b], Huynh-Bach-Son-Long Nguyen[c]

[a]*Institute of Fundamental and Applied Sciences, Duy Tan University, 03 Quang Trung, Danang city, Vietnam, email: dinhvanphuc82@gmail.com*
[b]*Department of Natural Science, Dong Nai University, No.04, Le Quy Don Street, Bien Hoa City, Dong Nai Province, Vietnam*
[c]*Faculty of Chemical and Environmental Engineering, Lac Hong University, 10 Huynh van Nghe Street, Buu Long Ward, Bien Hoa, Dong Nai, Vietnam*

Received 15 March 2018; Accepted 27 November 2018

ABSTRACT

In this work, α-MnO_2 and γ-MnO_2 nanomaterials are used to remove methylene blue (MB) from aqueous solution. Factors affecting the adsorption of MB on both materials are investigated, such as pH, adsorption time, and initial concentration of MB. The maximum adsorption of MB is obtained at pH = 8 after 80 min for γ-MnO_2 and pH = 9 after 150 min for α-MnO_2. Adsorption isotherm studies show that the adsorption monolayer capacity calculated from Langmuir models of γ-MnO_2 is higher than α-MnO_2 nanomaterial. Energy values calculated from Temkin and Dubinin–Radushkevich show that the uptake of MB on both α- and γ-MnO_2 materials is a physical process. Kinetic studies propose that the adsorption of MB on both α- and γ-MnO_2 materials follows the pseudo-second-order models. The results suggest that γ-MnO_2 nanomaterial can be used as an effective, low-cost adsorbent for the removal of MB from aqueous solution.

Keywords: γ-MnO_2 nanomaterial; α-MnO_2 nanomaterial; Methylene blue (MB); Adsorption

1. Introduction

Dyes and pigments are the main organic pollutant compounds in effluents released from various industries, especially the textile dyeing and processing factories. The presence of dyes in aqueous solution is very harmful to human beings and microorganisms even at low concentrations. Although methylene blue (MB) is a cationic dye which has a great number of applications in chemistry, biology, medical science, and dyeing industries, its long-term exposure can cause vomiting, nausea, anemia, and hypertension [1,2]. Thus, the treatment of wastewater containing such dyes and pigments is of interest owing to its harmful impacts on receiving waters [3].

A variety of physicochemical methods have been used to remove dye contaminants from wastewater, such as adsorption, flocculation, advanced oxidation processes, ozonation, membrane filtration, and biological treatment. The advantages and disadvantages of these methods have been extensively reviewed [4]. Among these techniques, adsorption is a promising method attracting scientists due to its high enrichment efficiency and the ease of phase separation [3–8].

Owing to various crystalline and morphologies, MnO_2 nanomaterials have been studied and applied for many areas, such as catalysts, electron materials, batteries, and adsorption [5,6,9–11]. In our previous researches, α- and γ-MnO_2 materials have been used to remove toxic heavy metal ions from aqueous solution [9–11]. Results show that these materials have large surfaces and are good for removing toxic heavy metal ions from aqueous solution with high efficiency. In this work, our goal is to compare the uptake of MB onto α- and γ-MnO_2 from aqueous solution in optimal condition by using

* Corresponding author.

Presented at the 2017 International Environmental Engineering Conference & Annual Meeting of the Korean Society of Environmental Engineers (IEEC 2017), 15–17 November 2017, Jeju, Korea.

five nonlinear models: Langmuir, Freundlich, Sips, Temkin, and Dubinin–Radushkevich, and three kinetic models: pseudo-first-order, pseudo-second-order, and intraparticle diffusion models. Additionally, the mechanism of the uptake of MB on these materials will be discussed. Finally, the better material for removing MB in effluent will be proposed.

2. Materials and methods

2.1. Materials

γ-MnO_2 and α-MnO_2 are synthesized via the reaction between $KMnO_4$ and C_2H_5OH as described in our previous reports [9,10]. Saturated $KMnO_4$ solution of 50 mL (3.0 g of $KMnO_4$ in 50 mL of double-distilled water) is gradually added into 150 mL of the mixture of 100 mL of C_2H_5OH and 50 mL of H_2O. The mixture is then strongly agitated for 8 h at room temperature to obtain γ-MnO_2 nanomaterial. α-MnO_2 nanomaterial is formed by calcining γ-MnO_2 at 600°C.

MB used as an adsorbate was prepared by dissolving MB (solid phase) in double-distilled water. Chemical structure and the ultraviolet (UV)-Vis absorption spectrum of the MB in solution are shown in Fig. 1. Three characteristic peaks (245, 292, and 664 nm) of MB are observed similar to those reported previously [12].

2.2. Instruments

The morphology of materials is investigated by ultrahigh-resolution scanning electron microscopy S – 4800 (SEM), and the surface area and pore size of the materials are determined by Brunauer–Emmett–Teller (BET) and Barrett–Joyner–Halenda (BJH) theories.

The pH values at the point of zero charge (pH_{PZC}) of γ-MnO_2 and α-MnO_2 nanomaterials are determined by using salt addition method [13]. Here, 0.200 g of each γ-MnO_2 or α-MnO_2 nanomaterial is added to 50.0 mL of 0.1M KNO_3 in ten 100-mL plastic beakers. The pH values are adjusted using a pH meter (MARTINI Instruments Mi-150, Romania) from 2 to 11 (±0.1) with 0.1M HNO_3 or 0.1M NaOH as needed in each beaker. These are then shaken for 24 h to obtain the equilibrium. After this period, each resulting pH is measured and the plot of initial pH (pHi) versus the difference between the initial and final pH values (DpH) is plotted. The PZC is taken as the point where pH = 0.

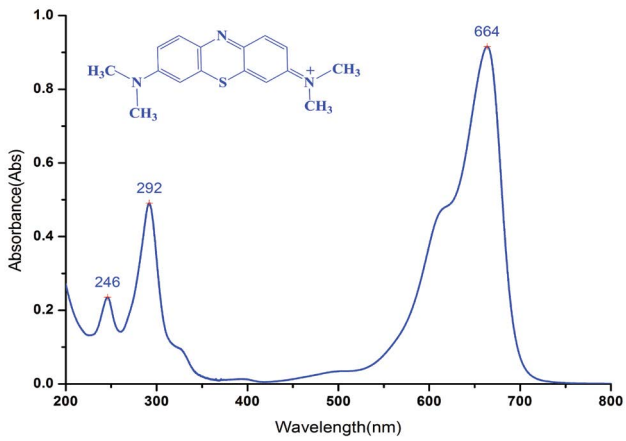

Fig. 1. UV-Vis absorption spectra of the MB solution.

Infrared spectra of these materials before and after the adsorption recorded over the wave number range of 4,000 to 400 cm^{-1} have been taken on a Fourier transform infrared (FTIR) spectroscopy (Perkin Elmer, Spectrum GX-FTIR, USA).

UV-Vis Spectrophotometer (V-630 made in Japan by Jasco) is used to determine the concentration of MB before and after the adsorption.

The pH measurements are done using a pH meter (MARTINI Instruments Mi-150, Romania); the pH meter is standardized using HANNA Instruments buffer solutions with pH values of 4.01 ± 0.01, 7.01 ± 0.01, and 10.01 ± 0.01.

A temperature-controlled shaker (Model IKA R5) is used for equilibrium studies.

2.3. Methods

The batch method is used to study the adsorption of MB on both materials. A 0.1 g of the nanomaterials is placed into a 100-mL conical flask containing 50 mL MB. The influences of pH, adsorption time, and initial MB concentrations are studied. Concentrations of MB before and after the adsorption are determined by UV-Vis method at 664 nm of the wavelength.

The percentage of removal and the adsorption capacity (q_e) are calculated using the mass balance equations as follows:

$$\%\text{Removal} = \frac{(C_0 - C_e)}{C_0} \times 100\% \quad (1)$$

$$q_e = \frac{(C_0 - C_e)}{m} \times V \quad (2)$$

where C_0 and C_e are the initial and equilibrium concentrations (mg/L), respectively.

2.4. Data analysis and model fitness

Five nonlinear isotherm models (Langmuir, Freundlich, Sips, Temkin, and Dubinin–Radushkevich) (Table 1) and three kinetic models (pseudo-first-order, pseudo-second-order, and intraparticle diffusion models) are fitted to the experimental data to investigate the nature of the adsorption [14]. All nonlinear isotherm parameters are evaluated and optimized by nonlinear regression using Origin 8.5.1 software.

3. Results and discussion

3.1. Characterization of γ-MnO_2 and α-MnO_2

Surface properties affecting the ability of adsorption of both materials are determined by SEM (Fig. 2) and transmission electron microscopy (TEM) (Fig. 3) and *BET* and BJH theories. Comparison of SEM and TEM images between γ-MnO_2 and α-MnO_2 materials shows that the α-MnO_2 nanomaterial consists of a large number of nanorods, whereas γ-MnO_2 nanomaterial possesses a porous surface including many nanospheres, which are smaller than the nanorods.

Table 1
Nonlinear isotherm models and meaning of nonlinear parameters

Isotherm	Nonlinear forms	Meaning of nonlinear parameters
Langmuir	$q_e = \frac{Q_L \times K_L \times C_e}{1 + K_L \times C_e}$	q_e: the adsorption capacity at equilibrium (mg/g) Q_L: the monolayer maximum adsorption capacity (mg/g) C_e: the equilibrium concentration (mg/L) K_L: Langmuir constant
Freundlich	$q_e = K_F \times C_e^{1/n}$	K_F: Freundlich constant n: adsorption intensity
Sips	$q_e = \frac{Q_S \times C_e^{\beta_S}}{1 + K_S \times C_e^{\beta_S}}$	Q_S: the maximum adsorption capacity (mg/g) K_S: Sips isotherm model constant (L/mg) β_s: Sips isotherm model exponent
Temkin	$q_e = \frac{RT}{b_T} \times \mathrm{Ln}\left(K_T C_e\right)$	K_T: Temkin isotherm equilibrium binding constant (L/g) β_T: Temkin isotherm constant
Dubinin–Radushkevich	$q_e = Q_{D-R} \times e^{\left(-\beta \times \varepsilon^2\right)}$	$Q_{D\text{-}R}$: the *D-R* maximum adsorption capacity (mg/g) β: Dubinin–Radushkevich isotherm constant (mol²/kJ²) ε: Dubinin–Radushkevich isotherm constant E: mean free energy (kJ/mol)
		$R^2 = 1 - \frac{\sum_{n=1}^{n}\left(q_{e,\mathrm{meas}} - q_{e,\mathrm{calc}}\right)^2}{\sum_{n=1}^{n}\left(q_{e,\mathrm{meas}} - \overline{q_{e,\mathrm{calc}}}\right)^2}$: correlation coefficient RMSE=$\sqrt{\frac{1}{n-1}\sum_{n-1}^{n}\left(q_{e,\mathrm{meas}} - q_{e,\mathrm{calc}}\right)^2}$: Root mean square error $\chi^2 = \sum_{n=1}^{n}\frac{\left(q_{e,\mathrm{meas}} - q_{e,\mathrm{calc}}\right)^2}{q_{e,\mathrm{calc}}}$: Nonlinear chi-square test

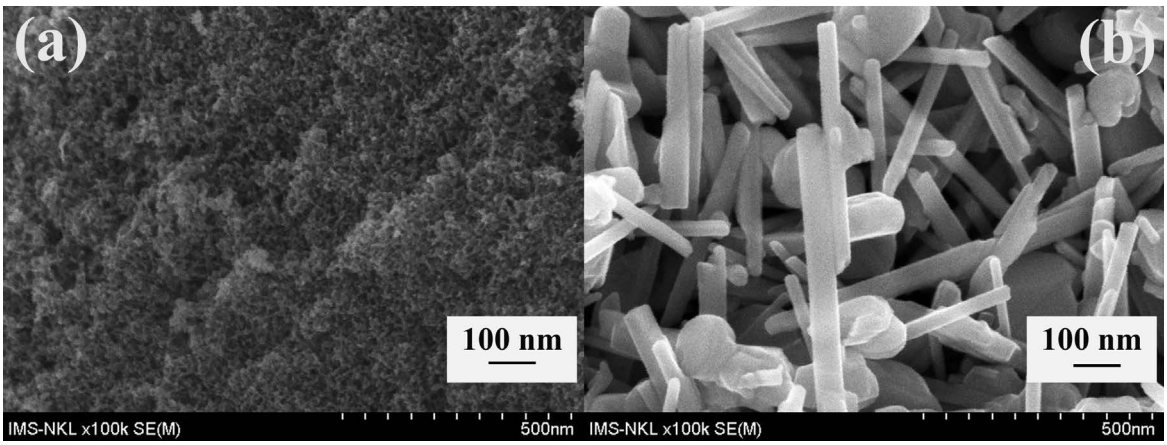

Fig. 2. (a) SEM images of γ-MnO_2 and (b) α-MnO_2 [11].

As a result, adsorption sites are formed on the γ-MnO_2 more than α-MnO_2 nanomaterial. In addition, both materials are mesoporous materials because of the average pore widths with diameters between 2 and 50 nm. Moreover, the surface area of γ-MnO_2 was 65.00 m^2/g, which was approximately 6.5 times more than that of α-MnO_2 (about 9.37 m^2/g). It can be predicted that the adsorption properties of γ-MnO_2 are more favorable than α-MnO_2.

Fig. 4 shows the FTIR spectra of γ-MnO_2 and α-MnO_2 nanomaterials. As can be seen, there are specific peaks of γ-MnO_2 nanomaterial in Fig. 4(a), including 3,451, 1,631, 1,535, and 1,413 cm^{-1} corresponding to physical and chemical water molecules in the structure of these materials and 522 cm^{-1} correlated with Mn–O bonding. However, these above specific peaks of water molecules disappeared when α-MnO_2 is formed from γ-MnO_2 at 600°C. Thus, there are

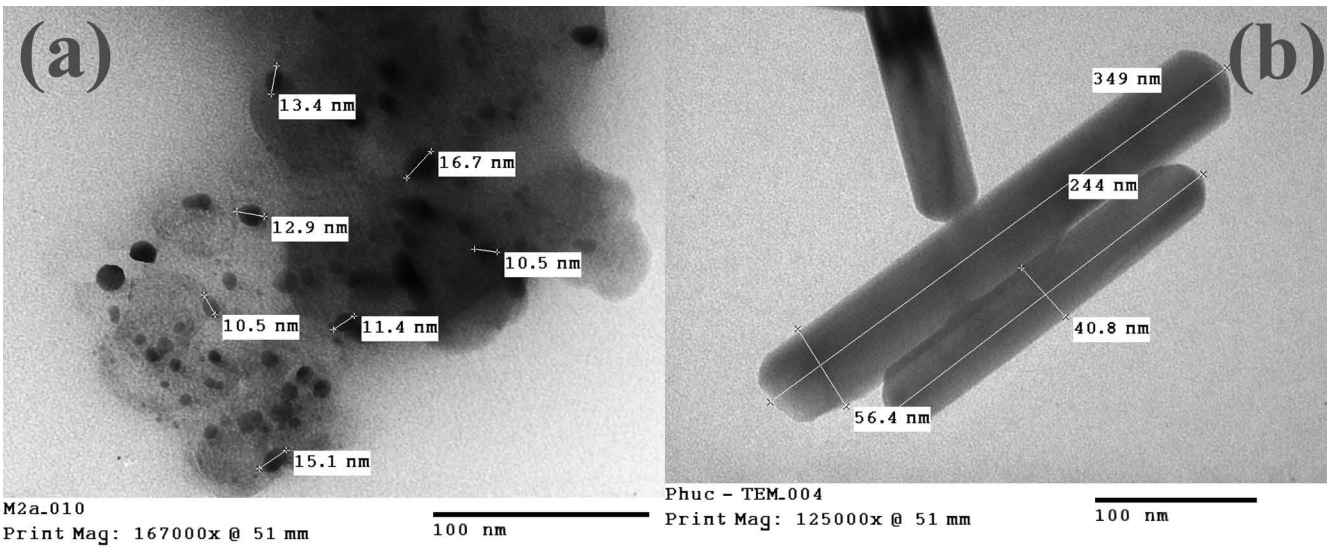

Fig. 3. (a) TEM images of γ-MnO_2 and (b) α-MnO_2 [11].

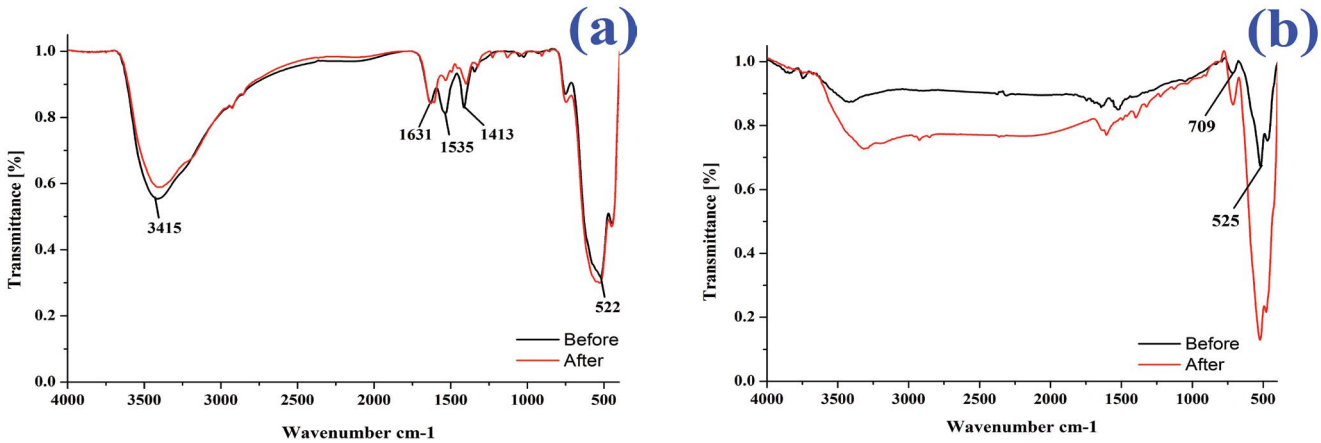

Fig. 4. FTIR spectrum of γ-MnO_2 (a) and α-MnO_2 (b) before and after the adsorption of MB.

two unique peaks of Mn–O bonding at 109 and 525 cm^{-1} that appeared in the FTIR spectra of α-MnO_2 as shown in Fig. 4(b).

pH_{PZC} is the value of pH at which the charge of surface obtains zero. If the pH values of solution are smaller than pH_{PZC} value ($pH < pH_{PZC}$), the adsorption sites will be protonated and the surfaces of these materials will be positively charged, through the ease of the adsorption of anion [Eq. (3)]. In contrast, when pH values of solution are higher than pH_{PZC} value ($pH > pH_{PZC}$), the surfaces of these materials are negatively charged that are more favorable for the uptake of cation [Eqs. (4) and (5)] [13,15–17]. In this work, pH_{PZC} values of γ-MnO_2 and α-MnO_2 are approximately 7.30 and 8.50, respectively (Fig. 5).

$$MOH_{(surf)} + H^+_{(aq)} = MnOH^+_{2(surf)} \quad (3)$$

$$MOH_{(surf)} + OH^-_{(aq)} = MnOOH^-_{(surf)} \quad (4)$$

$$MOH_{(surf)} + OH^-_{(aq)} = MnO^-_{(surf)} + H_2O \quad (5)$$

3.2. Factors affecting the removal of MB by γ-MnO_2 and α-MnO_2

Figs. 6(a) and (b) show the influence of pH on the uptake of MB by γ-MnO_2 and α-MnO_2 nanomaterials. As can be seen, there are fluctuations in the adsorption percentage of MB while pH values are changing. The maximum adsorption of MB is obtained at pH = 8 for γ-MnO_2 with nearly 96.96% of the removal and pH = 9 for α-MnO_2 with about 47.47% of the uptake. These results can be explained when the pH_{PZC} of γ-MnO_2 and α-MnO_2 nanomaterials are 7.3 ± 0.1 and 8.5 ± 0.1, respectively (Figs. 6(a) and (b)). Hence, when pH values of solution are higher than pH_{PZC}, the surfaces of γ-MnO_2 and α-MnO_2 nanomaterials are negative and acid Bronsted which are satisfied with the adsorption of cation as MB [13,15–17].

Fig. 7 shows the influence of time on the adsorption of MB on γ-MnO_2 and α-MnO_2. The uptake of MB by both γ-MnO_2 and α-MnO_2 nanomaterials increases with the increase in the adsorption time. These results can be determined via the decrease in the intensity of absorbance versus the adsorption time. However, γ-MnO_2 nanomaterial removes MB from aqueous solution better than α-MnO_2

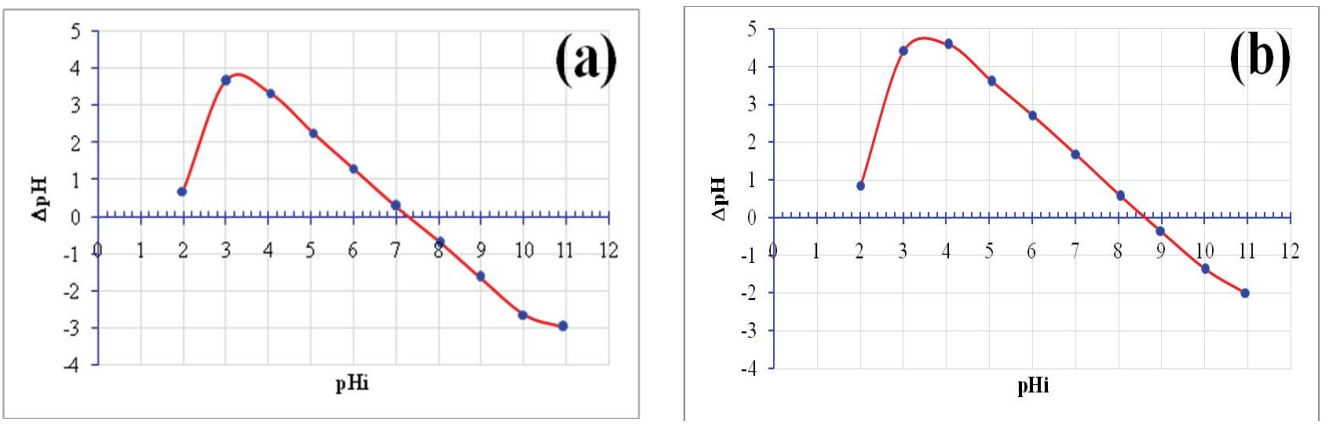

Fig. 5. pH values of the point of zero charge of γ-MnO_2 (a) and α-MnO_2 (b).

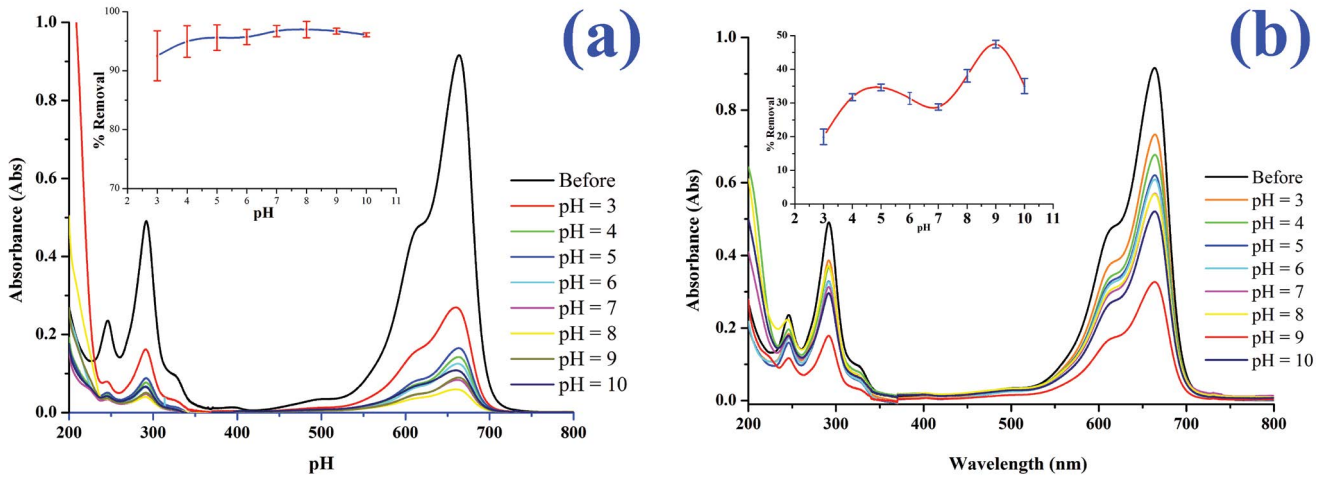

Fig. 6. Effect of pH on the removal of MB by γ-MnO_2 (a) and α-MnO_2 (b). Symbols with error bars indicate means ± *t*.SE (n = 3, P = 95%) (C_0 = 200 mg/L; shaking speed = 240 rpm, adsorption time = 180 min).

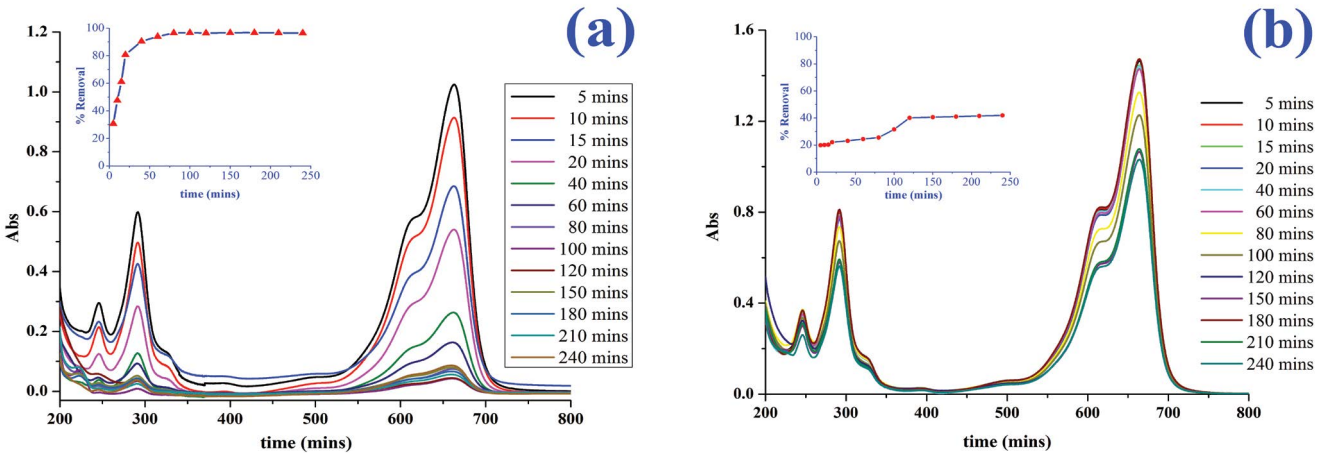

Fig. 7. Effect of time on the removal of MB by γ-MnO_2 (a) and α-MnO_2 (b) (C_0 = 200 mg/L; shaking speed = 240 rpm, pH = 8 for γ-MnO_2 and pH = 9 for α-MnO_2).

nanomaterial at different times. The adsorption of MB on γ-MnO_2 reaches the equilibrium after 80 min with over 96.53% of removal, whereas the uptake of MB by α-MnO_2 reaches the equilibrium after 150 min with roughly 40.6% of removal. These can be explained when the uptake of MB onto γ-MnO_2 nanomaterial surface occurred and obtained rapidly the equilibrium more than α-MnO_2 because this material possesses more adsorption sites than α-MnO_2 nanomaterials. In addition, there is not any shift at specific peaks which informs that the adsorption of MB on MnO_2 nanomaterials is unique. This mechanism is different from the researches of Zhang et al. [5] and Kuan et al. [6] who proposed that MB was not only adsorbed onto MnO_2 material surface but also partially oxidatively degraded to other organic compounds.

3.3. Adsorption isotherm studies

In order to understand the nature of adsorption of MB on γ-MnO_2 and α-MnO_2, five nonlinear isotherm models, Langmuir, Freundlich, Sips, Temkin, and Dubinin–Radushkevich [14], are used to fit the experimental data. Plots of these models are shown in Fig. 8, and nonlinear parameters are presented in Table 2.

By comparing error function parameters between γ-MnO_2 and α-MnO_2, it concludes that the experimental data of the removal of MB on γ-MnO_2 fit to five nonlinear isotherm models better than α-MnO_2 due to higher R^2 values, smaller root mean square error, and smaller χ^2 values. Sips model gives the best fit to experimental data for both γ-MnO_2 and α-MnO_2 nanomaterials. This can be explained that this model which is an empirical equation with three adjustable parameters consists of a combination of the Langmuir and Freundlich isotherm models and cannot be limited by adsorbate concentrations [11].

The n values which are obtained from Freundlich models within the present work are about 3.52 and 2.42 corresponding to γ-MnO_2 and α-MnO_2 nanomaterials, respectively. The latter indicates that MB can be easily adsorbed by both γ-MnO_2 and α-MnO_2 nanomaterials

Table 2
Nonlinear isotherm equilibrium parameters

Isotherm	Isotherm parameters		
		g-MnO_2	a-MnO_2
Langmuir	K_L	0.16	0.011
	Q_L (mg/g)	142	59
	RMSE	4.175	4.295
	R^2	0.9847	0.8299
	χ^2	1.955	4.341
Freundlich	n	3.52	2.42
	K_F	40.6	4.47
	RMSE	8.035	5.179
	R^2	0.9526	0.7527
	χ^2	4.943	6.165
Sips	Q_S	30.6	4.47
	K_S	0.1942	7.88×10^{-18}
	β_s	0.7769	0.4132
	RMSE	2.638	2.358
	R^2	0.9949	0.9487
	χ^2	0.6988	1.209
Temkin	K_T (L/mg)	2.32	0.08
	b_T (kJ/mol)	0.37	0.67
	RMSE	4.079	4.463
	R^2	0.9878	0.8163
	χ^2	1.284	4.264
Dubinin–Radushkevich	$Q_{D\text{-}R}$ (mg/g)	114	44
	β	1.72	431
	E (kJ/mol)	0.54	0.03
	RMSE	17.44	2.289
	R^2	0.7768	0.9516
	χ^2	41.64	1.132

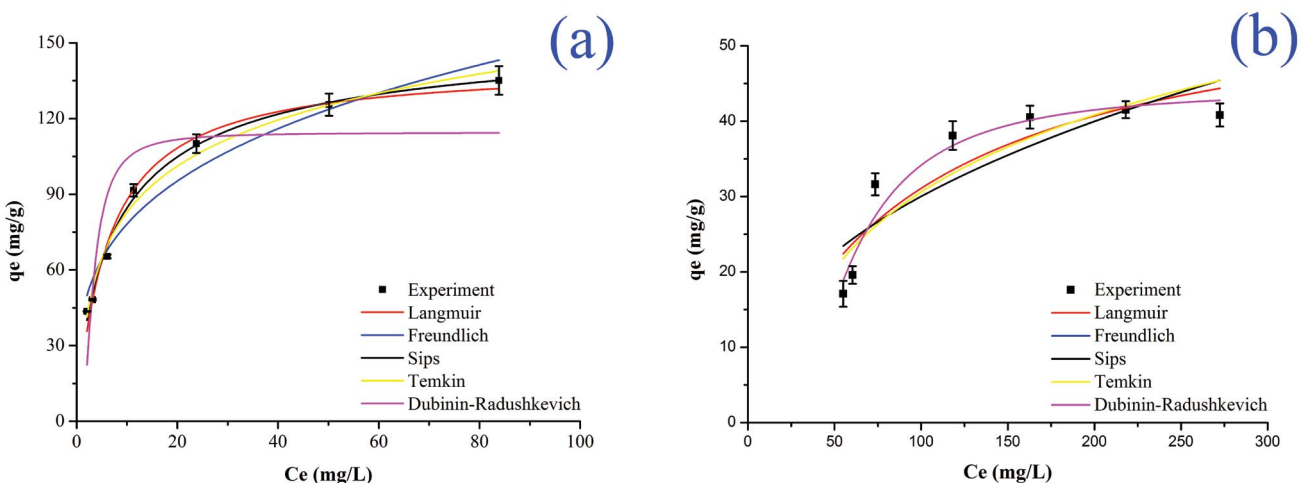

Fig. 8. Plots of nonlinear isotherm models of the adsorption of MB on γ-MnO_2 (a) and α-MnO_2 (b). Symbols with error bars indicate mean ± t.SE (n = 3, P = 95%) (shaking speed = 240 rpm, pH = 8 for γ-MnO_2 and pH = 9 for α-MnO_2, adsorption time = 180 min).

[18,19]. However, the maximum monolayer capacity (Q_L) calculated from the Langmuir isotherm equation of γ-MnO_2 (142 mg/g) is approximately three times more than α-MnO_2 (59 mg/g). It can be explained that γ-MnO_2 has a surface area of approximately 6.5 times more than that of α-MnO_2.

Energy values calculated from Temkin and Dubinin–Radushkevich models were found to be less than 8 kJ/mol provided that the uptake of MB onto α-MnO_2 and γ-MnO_2 is essentially a physical process [19,20]. These results can be confirmed and verified based on FTIR spectra of γ-MnO_2 (Fig. 4(a)) and α-MnO_2 (Fig. 4(b)) before and after the adsorption of MB. It is clear that there are no new peaks formed after the uptake of MB on the surface of both materials. However, the changes in intensity of specific peaks of γ-MnO_2 (1,535 and 1,413 cm^{-1}) and α-MnO_2 (709 and 525 cm^{-1}) conclude that these peaks are main adsorption sites of these materials.

3.4. Adsorption kinetic studies

The kinetics of the adsorption of MB on γ- and α-MnO_2 are analyzed by using different kinetic models such as pseudo-first-order, pseudo-second-order, and intraparticle diffusion models (Fig. 9). Formulas of three kinetic models and kinetic parameters are listed in Table 3.

Results show that the correlation coefficient R^2 values for pseudo-second-order model for both materials are higher than pseudo-first-order ones. In addition, the $q_{e,\text{cal}}$ values calculated from pseudo-first-order model are not as close to the experimental values ($q_{e,\text{exp}}$), whereas $q_{e,\text{cal}}$ values calculated from pseudo-second-order model satisfied with the experimental values ($q_{e,\text{exp}}$). All things considered, the adsorption of MB onto both materials is controlled by the pseudo-second-order model.

On the other hand, the pseudo-first-order and pseudo-second-order models are not able to identify the

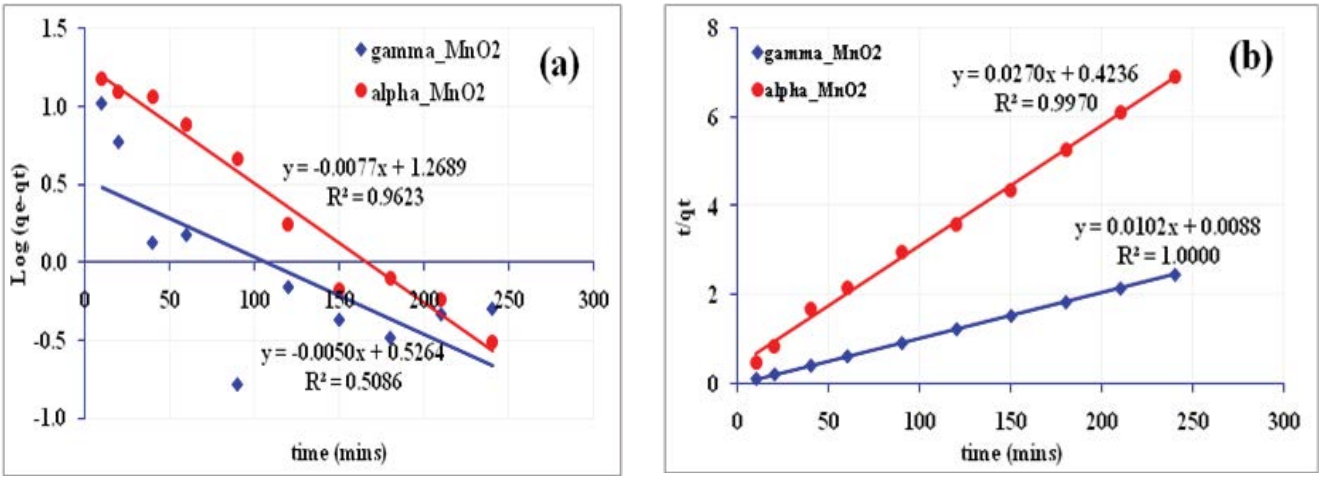

Fig. 9. Plots of pseudo-first-order kinetic (a) and pseudo-second-order kinetic (b) for the adsorption of MB onto γ- and α-MnO_2 (C_0 = 200 mg/L; shaking speed = 240 rpm, pH = 8 for γ-MnO_2 and pH = 9 for α-MnO_2).

Table 3
Models and kinetic parameters

Kinetic models		kinetic parameters	α-MnO_2	γ-MnO_2
		$q_{e\,(\text{exp})}$ (mg/g)	35 mg/g	98 mg/g
Pseudo-first-order model	$\log(q_e - q_t) = \log q_e - \frac{K_1 t}{2{,}303}$	K_1 (1/min)	0.018	0.012
		R^2	0.9623	0.5086
		$q_{e\,(\text{cal})}$ (mg/g)	18.57	3.36
Pseudo-second-order model	$\frac{t}{q} = \frac{1}{K_2 q_e^2} + \left(\frac{1}{q_e}\right) \times t$	K_2 (g/mg/min)	0.0017	0.0118
		R^2	0.9970	1.0000
		$q_{e\,(\text{cal})}$ (mg/g)	37.04	98.04
Intraparticle diffusion	$q_t = k_d t^{1/2} + C$	k_{d1}	1.6274	2.3207
		k_{d2}	0.1744	0.0097

q_e: the amount of solute adsorbed at equilibrium per unit weight of adsorbent (mg/g); q: the amount of solute adsorbed at any time (mg/g); K_1, K_2: the adsorption constants; t: adsorption time.

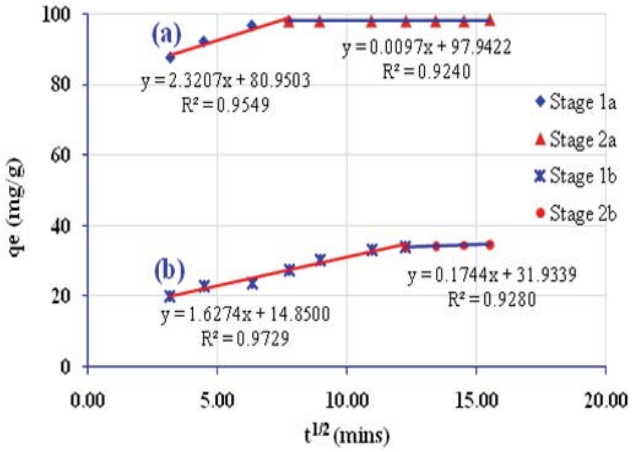

Fig. 10. Plots of intraparticle diffusion models for the adsorption of MB onto γ-MnO_2 (a) and α-MnO_2 (b).

diffusion mechanisms. Thus, the intraparticle diffusion model developed by Weber and Morris [21] is utilized in order to determine the diffusion mechanism involved in the adsorption process. This model is based on the following equation [21]:

$$q_t = k_d t^{1/2} + C \tag{6}$$

where C characterizes the effects caused by the boundary layer. The results obtained within this model are shown in Fig. 10. These results clearly indicate that the uptake of MB on both material surface is likely to occur throughout two stages. In the first stage, MB particles are quickly transferred from the solution to the boundary film of the particles (bulk diffusion) within about 80 min for γ-MnO_2 and 150 min for α-MnO_2. In the second stage, a gradual adsorption occurred because of the main reason that the concentration of MB in the solution is extremely low as well as the number of adsorption sites decreases [22]. Additionally, it is seen that the plot of q_t versus $t^{1/2}$ obtained within this first stage does not pass through the origin and the presence of the boundary layer effect characterized by the nonzero value of C. These results indicate that the uptake follows not only the intraparticle diffusion but also two or more different diffusion mechanisms [23]. The values of the diffusion constants (k_{d1}, k_{d2}) obtained within all three stages are listed in Table 3.

4. Conclusions

The removal of MB using α- and γ-MnO_2 nanomaterials is investigated. Sips model gives the best fit to the experimental data for both materials. Energy values calculated from Temkin and Dubin-Radushkevich indicate that the uptake of MB on α- and γ-MnO_2 nanomaterials is physical process. The pseudo-second-order kinetic models describe the adsorption of MB on both materials better than the pseudo-first-order kinetic models. Results show that γ-MnO_2 nanomaterial removes MB from aqueous solution better than α-MnO_2; hence, γ-MnO_2 nanomaterial will be satisfied material for the treatment of MB from wastewater.

References

[1] D. Pathania, S. Sharma, P. Singh, Removal of methylene blue by adsorption onto activated carbon developed from Ficus carica bast, Arab. J. Chem., 10 (2017) S1445–S1451.
[2] Y. He, D.B. Jiang, J. Chen, D.Y. Jiang, Y.X. Zhang, Synthesis of MnO_2 nanosheets on montmorillonite for oxidative degradation and adsorption of methylene blue, J. Colloid Interface Sci., 510 (2018) 207–220.
[3] M. Rafatullah, O. Sulaiman, R. Hashim, A. Ahmad, Adsorption of methylene blue on low-cost adsorbents: a review, J. Hazard. Mater., 177 (2010) 70–80.
[4] M.A.M. Salleh, D.K. Mahmoud, W.A.W.A. Karim, A. Idris, Cationic and anionic dye adsorption by agricultural solid wastes: a comprehensive review, Desalination, 280 (2011) 1–13.
[5] W. Zhang, Z. Yang, X. Wang, Y. Zhang, X. Wen, S. Yang, Large-scale synthesis of β-MnO_2 nanorods and their rapid and efficient catalytic oxidation of methylene blue dye, Catal. Commun., 7 (2006) 408–412.
[6] W.H. Kuan, C.Y. Chen, C.Y. Hu, Removal of methylene blue from water by γ-MnO_2, Water Sci. Technol., 64 (2011) 899–903.
[7] L. Borah, M. Goswami, P. Phukan, Adsorption of methylene blue and eosin yellow using porous carbon prepared from tea waste: adsorption equilibrium, kinetics and thermodynamics study, J. Environ. Chem. Eng., 3 (2015) 1018–1028.
[8] J. Chang, J. Ma, Q. Ma, D. Zhang, N. Qiao, M. Hu, H. Ma, Adsorption of methylene blue onto Fe_3O_4/activated montmorillonite nanocomposite, App. Clay Sci., 119 (2016) 132–140.
[9] L.N. Chung, D. Van Phuc, Sorption of lead (II), cobalt (II) and copper (II) ions from aqueous solutions by γ-MnO_2 nanostructure, Adv. Nat. Sci. Nanosci. Nanotechnol., 6 (2015) 025014.
[10] V.-P. Dinh, N.-C. Le, T.-P.-T. Nguyen, N.-T. Nguyen, Synthesis of α-MnO_2 nanomaterial from a precursor γ-MnO_2: characterization and comparative adsorption of Pb(II) and Fe(III), J. Chem., 2016 (2016) 9.
[11] V.-P. Dinh, N.-C. Le, T.-D. Le, T.-A. Bui, N.-T. Nguyen, Comparison of the adsorption of Fe(III) on alpha- and gamma-MnO_2 nanostructure, J. Electron. Mater., 46 (2017) 3681–3688.
[12] X. Yu, L. Huang, Y. Wei, J. Zhang, Z. Zhao, W. Dai, B. Yao, Controllable preparation, characterization and performance of Cu_2O thin film and photocatalytic degradation of methylene blue using response surface methodology, Mater. Res. Bull., 64 (2015) 410–417.
[13] A.M. Cardenas-Peña, J.G. Ibanez, R. Vasquez-Medrano, Determination of the point of zero charge for electrocoagulation precipitates from an iron anode, Int. J. Electrochem. Sci., 7 (2012) 6142–6153.
[14] K.Y. Foo, B.H. Hameed, Insights into the modeling of adsorption isotherm systems, Chem. Eng. J., 156 (2010) 2–10.
[15] T. Mahmood, M.T. Saddique, A. Naeem, P. Westerhoff, S. Mustafa, A. Alum, Comparison of different methods for the point of zero charge determination of NiO, Ind. Eng. Chem. Res., 50 (2011) 10017–10023.
[16] M. Gheju, I. Balcu, G. Mosoarca, Removal of Cr(VI) from aqueous solutions by adsorption on MnO_2, J. Hazard. Mater., 310 (2016) 270–277.
[17] M. Singh, D.N. Thanh, P. Ulbrich, N. Strnadová, F. Štěpánek, Synthesis, characterization and study of arsenate adsorption from aqueous solution by α- and δ-phase manganese dioxide nanoadsorbents, J. Solid State Chem., 183 (2010) 2979–2986.
[18] T.A. Saleh, A. Sarı, M. Tuzen, Effective adsorption of antimony(III) from aqueous solutions by polyamide-graphene composite as a novel adsorbent, Chem. Eng. J., 307 (2017) 230–238.
[19] V.-P. Dinh, N.-C. Le, L.A. Tuyen, N.Q. Hung, V.-D. Nguyen, N.-T. Nguyen, Insight into adsorption mechanism of lead(II) from aqueous solution by chitosan loaded MnO_2 nanoparticles, Mater. Chem. Phys., 207 (2018) 294–302.

[20] R.R. Bhatt, B.A. Shah, Sorption studies of heavy metal ions by salicylic acid–formaldehyde–catechol terpolymeric resin: isotherm, kinetic and thermodynamics, Arab. J. Chem., 8 (2015) 414–426.
[21] W.J. Weber, J.C. Morris, Kinetics of adsorption carbon from solutions, J. Sanit. Eng. Div., Proc. Am. Soc. Civ. Eng., 89 (1963) 31–60.
[22] F.-C. Wu, R.-L. Tseng, R.-S. Juang, Comparative adsorption of metal and dye on flake- and bead-types of chitosans prepared from fishery wastes, J. Hazard. Mater., 73 (2000) 63–75.
[23] S. Vasiliu, I. Bunia, S. Racovita, V. Neagu, Adsorption of cefotaxime sodium salt on polymer coated ion exchange resin microparticles: kinetics, equilibrium and thermodynamic studies, Carbohyd. Polym., 85 (2011) 376–387.